INTERNATIONAL JOURNAL FOR NUMERICAL METHODS IN FLUIDS, VOL. 9, 987–1009 (1989)

COMPARISON OF k–ε AND ALGEBRAIC REYNOLDS STRESS MODELS FOR SWIRLING DIFFUSER FLOW

S. W. ARMFIELD

Centre for Water Research, University of Western Australia, Nedlands, Western Australia 6009

AND

C. A. J. FLETCHER

University of Sydney, Sydney, Australia 2006

SUMMARY

A brief overview of classes of turbulent swirling flow in conical diffusers is given, together with a description of appropriate numerical schemes for each class. Numerical results obtained for the class of moderate swirl in a 20° diffuser and for the class of no swirl in an 8° diffuser are compared with experimental results. The results are obtained using a multi-sweep scheme solving the full steady state time-averaged Navier–Stokes equations. Turbulence quantities are approximated using two types of algebraic Reynolds stress model and two types of k–ε model. One of the algebraic Reynolds stress models includes extra production terms associated with the Christoffel symbols in cylindrical co-ordinates, and one of the k–ε models includes a swirl-related modification to the ε equation. It is demonstrated that the standard k–ε model gives poor prediction of the mean flow, and it is necessary to at least use the modified form or one of the two algebraic Reynolds stress models.

KEY WORDS Turbulence Swirl Conical diffusers Multi-sweep Navier–Stokes equations Reynolds stress mode k–ε model

1. INTRODUCTION

Diffusers are commonly used fluid mechanical devices which act to convert dynamic pressure to static pressure. When placed in the flow downstream of the rotor in a wind turbine, they increase the amount of energy that may be extracted from the windstream.[1,2] A measure of the efficiency of the diffuser in performing this function is the total pressure recovery obtained. For conical diffusers it is found that maximum pressure recovery is obtained for total internal angles of around 8°, provided the area ratio is large enough, typically around four.[3]

It is not always practical to use such an optimum diffuser because of design constraints, such as size and weight, and for this reason it is useful to know if it is possible to obtain near-optimum pressure recovery for smaller, lighter diffusers. Thus, typically, it is desired to use a wider-angle diffuser to reduce the total length and the amount of material required. However, when a wider-angle diffuser is used with an area ratio of four, the occurrence of separation at the wall at a downstream location will substantially reduce the pressure recovery. The separation is caused by the occurrence of a region of low momentum near the wall, due to the rapid increase in thickness of the boundary layer, interacting with the positive axial pressure gradient. In the extreme case

0271–2091/89/080987–23$11.50

Received 20 June 1988

the diffuser will fully stall, i.e. the flow will separate at the diffuser entrance, and there will be no pressure recovery at all. Thus the desire to reduce the weight and size of the diffuser must be balanced by the effect of the loss in pressure recovery, and therefore the loss in efficiency, that the use of wider-angle diffusers entails.

It has been found that the inclusion of swirl in the flow can prevent separation occurring for diffuser angles and area ratios at which it would otherwise occur.[4] In this way the presence of swirl may allow near-optimum pressure recovery to be obtained from effectively smaller and lighter diffusers. In many applications, such as that of the diffuser-augmented wind turbine mentioned above, the flow is already swirling. In these cases any increase in efficiency obtained for a given diffuser by the presence of swirl is entirely serendipitous.

The effect of including swirl is to produce a significant positive radial pressure gradient at the diffuser entrance, the result of the pressure balancing the centrifugal acceleration of the rotating component of the flow. The rapid decay of swirl in the diffuser leads to rapid decay in the radial pressure gradient. The effect of this is to produce a larger positive axial pressure gradient at the axis than would be the case for non-swirling flow and the same diffuser. This in turn leads to a drop in the axial centreline velocity, resulting in an increase in the near-wall axial velocity, due to the constant mass flow constraint, which acts to prevent the occurrence of separation at the wall. However, the presence of an excessive amount of swirl will cause the centreline axial velocity to drop so much that reversal occurs at the centreline, leading once again to a reduced pressure recovery.

In practice most flows that pass through a diffuser will be turbulent. It is therefore also necessary to consider the effect of turbulence on the mean flow structure, and the effect of the diffuser on the turbulence structure. Turbulence has a beneficial effect on the diffuser efficiency, in much the same way as swirl does, by acting to prevent the onset of separation. This is accomplished by the characteristic of turbulent velocity profiles being fuller than laminar velocity profiles in the boundary layer. The result of this is that the momentum in the near-wall region is larger and therefore better able to resist the positive pressure gradient.

The effect of the diffuser on the turbulence appears to be two-fold. Firstly it causes the near-wall peak in the turbulence quantities, which is very close to the wall in a developing boundary layer, to occur at a distance much further out from the wall. Secondly it acts to amplify the level of turbulence considerably (see Figures 9 and 10).

It is assumed that the flow is axisymmetric, of constant viscosity and incompressible. We have only considered diffusers with an area ratio of around four, which for turbulent flow are known to lead to optimal pressure recovery when the total internal angle is around 8°, and have assumed that the inlet flow consists of a thin developing boundary layer with an inviscid core. The aim has been to produce a code capable of satisfactorily predicting the mean flow quantities, which may then be used as an aid in the design of efficient diffusers.

It is useful to divide turbulent swirling diffuser flow into several regimes, on the basis of the appearance or otherwise of regions of separating and reversing axial velocity, and on the basis of the strength of the swirl.[5] The flow types, indicated in Table I, may be further classified as being of elliptic or parabolic type, based on the observed numerical behaviour of the flow prediction. Flows that are classified as parabolic are able to be simulated numerically using a single-sweep algorithm marching in the axial direction, i.e. they are soluble numerically as an initial value problem in space.[6] Those that are not, and therefore require some sort of multi-sweep algorithm, are classified as elliptic.

It has been found that for diffuser angles of less than 10° no separation at the wall occurs for non-swirling flow. For diffuser angles of between 10° and 20° separation will occur for non-swirling flow; however, it is possible by the inclusion of swirl to prevent the wall separation

Table I. Table of flow regimes; Θ is the diffuser half-angle

Diffuser/flow criterion	Characteristics	Flow type
$2\Theta < 10°$ Weak swirl ($Sn < 0{\cdot}3$)	No separation at the wall Small (< 10%) reduction in centreline axial velocity	Parabolic
$2\Theta < 10°$ Moderate swirl ($0{\cdot}3 < Sn < 0{\cdot}6$)	No separation at the wall Near-reversing centreline axial velocity	Elliptic
$10° < 2\Theta < 20°$ Weak swirl	Separation at the wall Small (< 10%) reduction in centreline axial velocity	Elliptic
$10° < 2\Theta < 20°$ Moderate swirl	No separation at the wall Near-reversing centreline axial velocity	Elliptic
$\Theta > 20°$ and/or strong swirl ($Sn > 0{\cdot}6$)	Separation at the wall and/or centreline axial velocity reversal	Elliptic

occurring. For diffuser angles of greater than 20° the amount of swirl necessary to prevent separation at the wall produces centreline reversal; that is, it is not possible to have a flow completely free of separation for diffuser angles of greater than 20°. We divide the swirl into three types based on the magnitude of its effect on the centreline axial velocity. Weak swirl leads to minimum reduction in the axial centreline velocity. Moderate swirl leads to a significant reduction in the centreline axial velocity, without producing reversal. Strong swirl leads to centreline axial velocity reversal.

The diffuser angle, area ratio and inlet swirl profile all influence the magnitude of the effect of the swirl on the axial velocity. The inlet swirl profile is either of the solid body rotation variety or, to some degree, of the free vortex type. It is found that generally the free vortex type of swirl will lead to a larger effect on the axial velocity than the solid body type for a given angular momentum. For this reason a meaningful swirl number Sn with which to categorize the effect of swirl on the axial velocity is the ratio of the maximum swirl velocity W^{max} to the mean axial velocity U^{mean} at the inlet. We then find that weak swirl typically has $Sn < 0.3$, moderate swirl has $0{\cdot}3 < Sn < 0{\cdot}6$ and strong swirl has $Sn > 0{\cdot}6$. This division of swirling conical diffuser flow is tabulated in Table I.

Three numerical schemes have been developed and tested on swirling diffuser flow. The equation types and flow regimes that each of the schemes is used for are summarized in Table II.

Table II. Table of numerical schemes

Numerical scheme	Flow type	Equation set
Single-sweep[6]	Parabolic	Reduced equations
Quasi-multi-sweep[8]	Parabolic	Partially reduced equations or reduced equations
Multi-sweep[9]	Elliptic or parabolic	Full equations or partially reduced equations or reduced equations

1.1. Single-sweep

The single-sweep scheme may only be used to solve a reduced form of the Navier–Stokes equations; that is, the Navier–Stokes equations with all the axial diffusion terms deleted, and additionally all the terms associated with the cross-stream velocity deleted from the cross-stream momentum equation, on an order-of-magnitude basis. In the rest of the paper U will be the axial or streamwise component of velocity, V the radial of cross-stream component and W the swirl.

In this scheme, presented in detail in Armfield and Fletcher,[6] the domain is swept once in the axial direction. At each axial location the values of all the variables are obtained in sequence from their governing equations using, where necessary, values of the variables at the previous axial location. The governing equations for each variable are as follows. U is obtained from the axial momentum equation, W from the circumferential momentum equation and V from the continuity equation. The pressure is split into two components, one of which is interpreted as being the pressure at the axis and the other the radial variation of pressure. The pressure at the axis is obtained by enforcing the mass flow constraint. The radial variation in pressure is related directly to the swirl via the reduced form of the radial momentum equation.

All equations are discretized using centred second-order differences for the linear terms. When non-linear terms are not available at the centred axial location, they are projected from upstream. This produces tridiagonal systems from the axial and circumferential momentum equations, and bidiagonal systems from the continuity equation and the radial momentum equation. The equations are then inverted in the following order at each axial location $x = x^n$. The discretized form of the circumferential momentum equation is inverted in two radial sweeps to give the new values of W at $x = x^{n+1}$. The radial pressure variation is obtained from the discretized form of the radial momentum equation, integrated in a single radial sweep. The axial momentum equation is integrated using the most recent value of the radial variation in pressure to obtain U^{n+1} implicitly in terms of the axial pressure variation. The axial pressure is then obtained from the mass flow constraint, and back substitution used to give U^{n+1}. V^{n+1} is obtained by integrating the continuity equation in a single radial sweep using the most recently calculated values of U^{n+1}. This process is repeated at each axial location, with the entire domain swept in a single downstream march.

When an attempt is made to use the single-sweep scheme to solve any equation set other than the reduced equations, an instability associated with the size of the marching step makes it impossible to obtain both sufficient resolution and a stable solution. This instability is discussed fully in Armfield and Fletcher.[7]

1.2. Quasi-multi-sweep

This scheme, described in detail in Armfield and Fletcher,[8] is used to solve the partially reduced equations; that is, the Navier–Stokes equations with only the axial diffusion terms deleted. It makes multiple sweeps of the domain and solves for all dependent variables except the pressure in exactly the same manner as the single-sweep scheme. The pressure is stored over the entire domain, allowing the pressure derivative in the axial momentum equation to be forward differenced, and the new values obtained during each sweep used to relax the stored field. The axial pressure is obtained by enforcing a mass flow constraint, also in the same manner as in the single-sweep scheme, while the radial variation in pressure is obtained from the discretized version of the radial momentum equation, integrated using a single radial sweep.

Thus, when the quasi-multi-sweep scheme is used, multiple sweeps of the domain are made, with only the pressure solution stored and relaxed, until a converged pressure solution is obtained. One final sweep of the domain may be made, using the converged pressure solution, to obtain the remaining variables. The quasi-multi-sweep scheme may be used to solve the reduced equations, but when it is used to solve the full equations a similar minimum step size stability restriction to that encountered when the single-sweep scheme is used to solve the full equations makes it difficult to obtain sufficient resolution and a stable solution.

It has been found that for swirling diffuser flows no advantage has been gained by using the quasi-multi-sweep scheme, since it has only been capable of simulating those flows that may also be simulated using the single-sweep scheme. For this reason development of this scheme has not been pursued.

1.3. Multi-sweep

This scheme is briefly described in Section 2.7. The results presented in Section 3 have been obtained using a multi-sweep scheme.

1.4. Numerical methods for strongly swirling flow

Strongly swirling diffuser flow, sufficient to cause axial flow reversal at the centreline, is fully elliptic and therefore has no dominant direction. For this reason none of the numerical methods developed in the current project and described above may be used to simulate it, as they all exploit the existence of a dominant flow direction to enable the use of a more efficient algorithm.

Researchers who have attempted to numerically predict strongly swirling flow have almost universally used the TEACH code produced at Imperial College[9] or a variant of it. The TEACH code itself is based on the SIMPLE scheme developed by Patankar and Spalding.[10] Thus we see for instance Kubo and Gouldin[11] use a modified form of Gosman's relaxation method, a precursor to TEACH. Rhode *et al.*[12] use a version of the TEACH-T computer program. Hah[13] uses a method he attributes to Gosman and Pun, with the same reference as that given by Kubo and Gouldin above, and therefore presumably uses TEACH. Leschziner and Rodi[14] use TEACH to simulate a strongly swirling free jet. Truelove and Mahmud[15] use a modification of the TEACH program also to simulate a strongly swirling jet flow.

All the TEACH-derived programs share the common features of using a SIMPLE scheme to enforce continuity and obtain the pressure field, a control volume approach to discretize the governing equations and under-relaxation with an ADI procedure to integrate the resulting discrete equations. Most development in recent years has centred around the differencing form for the convective terms. Initially hybrid central/upwind methods were used; however, recently more accurate methods have been employed—Truelove and Mahmud used a QUICK scheme

and Hah a skewed second-order scheme. A more complete discussion of the TEACH program, together with a comparison between it and the Multi-Sweep program used to obtain the results in the present paper, is given in Armfield and Fletcher.[16]

1.5. Turbulence models; overview

Three types of turbulence models have been developed and evaluated. The first of these is an algebraic eddy viscosity approach, similar to that of Cebeci and Smith.[17] In this method the eddy viscosity is related to the distance from the wall in the near-wall region and to the displacement thickness in other regions of the flow. Results obtained using the above method are presented in Armfield and Fletcher.[6]

The second is the two-equation k–ε model.[17] Models of this type are the most commonly used and evaluated in the field of turbulence simulation, and have been shown to give satisfactory mean flow predictions in many cases.[14,18] One of the areas in which the standard k–ε model is suggested to give unsatisfactory predictions is that of swirling jet flow.[19,20] Such poor prediction has been variously attributed to the inappropriate assumption of an isotropic eddy viscosity and to the commonly used form of the ε equation not being suitable for swirling flow. To attempt to rectify the second of these two problems, we have tested a swirl-related modification to the ε equation, given in Section 2.4, as well as the standard k–ε model. To deal with the other difficulty, that of a non-isotropic eddy viscosity, rather than adjusting the k–ε model, we have chosen to use an algebraic Reynolds stress model,[21] which is a direct approximation of the Reynolds stress equation, retaining their anisotropy.

When algebraic Reynolds stress models are used for swirling flow, it is generally assumed that extra terms arising from the convective components, but with the appearance of production terms, obtained when the equations are expressed in cylindrical co-ordinates, may be treated as production terms, given in Section 2.3.[22] In the current project we have compared results with and without these 'false' production terms included.

In the present paper we present results for a moderately swirling flow in a 20° diffuser, obtained using the multi-sweep scheme solving the full Navier–Stokes equations. We have used this flow as a means to test four turbulence models: two k–ε models and two algebraic Reynolds stress models. One k–ε model is the standard model, whilst the other includes a modification to allow for the effect of swirl on the turbulence parameters to be more accurately predicted. The difference between the two algebraic Reynolds stress models is the inclusion of the extra 'false' production terms. Some results are also presented for non-swirling flow in an 8° diffuser, where a more detailed comparison of the prediction of the turbulence quantities is made.

The derivation of the turbulence models is given in generalized co-ordinate-free tensor form in Section 2 and the equations are then expressed in a physical co-ordinate system, in this case in spherical co-ordinates. In Section 3 the results are presented, a discussion is provided in Section 4 and conclsions are given in Section 5.

2. GOVERNING EQUATIONS AND BOUNDARY CONDITIONS

The governing equations of Newtonian flow may be written in terms of $\underline{U}$, the mean velocity, and u, the fluctuating velocity vectors, in co-ordinate-free tensor form as

$$\rho \underline{U}^i_{,t} + \rho \underline{U}^k \underline{U}^i_{,k} + \rho \overline{(u^k u^i)}_{,k} = -g^{ik} P_{,k} + \mu g^{lk} U^i_{,lk} \tag{1}$$

and the continuity equation as

$$\underline{U}^i_{,i} = 0. \tag{2}$$

$\underline{U}$ is the velocity vector, P is the pressure, g is the metric tensor, μ is the dynamic viscosity and ρ is the density. Superscripts indicate contravariant quantities, subscripts indicate covariant quantities, apostrophes in the lower position indicate covariant derivatives and $_{,t}$ is the partial derivative with respect to time. The above equations are for fluid with constant density and viscosity and are in the contravariant form.

As can be seen in equation (1), the fluctuating components appear only in the term $\overline{\rho u^k u^i}$. These terms are the fluctuating velocity correlations; they are the components of a second-order tensor, generally called the Reynolds stress tensor, and are the Reynolds or turbulent stresses.

2.1. *Reynolds stress equations*

Equation (1) together with the continuity equation provides us with a system of four equations with ten unknowns: the three mean velocity components, pressure and the six Reynolds stress components. The system is therefore underdetermined and extra equations must somehow be obtained to close it. It is possible to derive additional partial differential equations for each of the Reynolds stresses.[5] When this is done we obtain the following equations:

$$\underbrace{\rho\overline{(u^iu^j)}_{;t}+{}^{E}\underbrace{\rho\underline{U}^k\overline{(u^iu^j)}_{,k}}_{\text{convection}}}_{\text{convection}}=\underbrace{-\underbrace{\rho\overline{u^iu^k}\underline{U}^j_{,k}-\rho\overline{u^ju^k}\underline{U}^i_{,k}}_{\text{production}}+\underbrace{\overline{p(g^{jk}u^i_{,k}+g^{ik}u^j_{,k})}}_{\text{pressure strain}}}$$

$$\underbrace{-\overline{\rho(u^ku^iu^j)}_{,k}+\mu g^{kl}\overline{(u^iu^j)}_{,kl}-\overline{g^{ik}(u^jp)}_{,k}-\overline{g^{jk}(u^ip)}_{,k}}_{\text{diffusion}}\underbrace{-2\mu g^{kl}\overline{(u^i_{,k}u^j_{,l})}}_{\text{dissipation}} \tag{3}$$

The labels are used to give a physical interpretation to each term and provide a convenient way of referring to components of the equation. Equation (3) is an exact set of equations for the Reynolds stresses; if they formed a soluble system, the search for a universal turbulence model would be over, but as is explained in the next section this is not the case.

Equation (3) may be used to construct an exact equation for $k=\overline{u^iu_i}/2$, the kinetic energy of the turbulent fluctuations, by contracting it on the free indices and dividing by two, giving

$$\underbrace{\rho k_{;t}+\underbrace{\rho\underline{U}^k k_{,k}}_{\text{convection}}}_{\text{convection}}=\underbrace{-\underbrace{\rho\overline{u^ku_l}U^l_{,k}}_{\text{production}}-\underbrace{\rho\overline{(u^kk)}_{,k}+\mu g^{kl}\overline{k}_{,kl}-\overline{g^{ik}(pu_i)}_{,k}}_{\text{diffusion}}-\underbrace{\mu g^{kl}\overline{(u^i_{,l}u_{i,k})}}_{\text{dissipation}}} \tag{4}$$

2.2. *Reynolds stress equations in modelled form*

Unfortunately, in constructing the additional Reynolds stress equations (3), new dependent variables have been introduced: the pressure strain term, the triple correlation and the pressure correlation in the diffusion term, and the dissipation term; so the system is still unclosed. Since in the present study an algebraic Reynolds stress model is used, it is only necessary to introduce modelling assumptions for the dissipation and pressure strain terms.

The dissipation is assumed to be isotropic and therefore evenly distributed between the three normal stresses, and thus able to be represented by a scalar, giving[17]

$$2\mu g^{kl}\overline{(u^i_{,k}u^j_{,l})}=\tfrac{2}{3}\rho g^{ij}\varepsilon.$$

The pressure strain term has been shown to consist of three components,[23] one of which, the wall echo term, is considered only to be significant in near-wall regions (Section 4.1) and is not included in the present model due to the use of a mixing length formulation in the near-wall

region, given in Section 2.5. The other two are the term arising from the mutual interaction of the fluctuating velocities and that arising from the interaction of the mean rate of strain with the turbulence. Rotta's proposal[24] is generally used to model the first of these. Several suggestions have been made for modelling the second term. The one used here was proposed by Naot *et al.*[25] and is used primarily because of its simplicity coupled with the fact that it appears to perform as well as the other suggestions.[26,27] This gives

$$\overline{p(g^{jk}u^i_{,k}+g^{ik}u^j_{,k})} = \underbrace{-\rho C_1 \varepsilon/k(\overline{u^iu^j}-\tfrac{2}{3}g^{ij}k)}_{\text{due to Rotta}} \underbrace{-\rho C_2(-u^iu^k\underline{U}^j_{,k}-\overline{u^ju^k}\,\underline{U}^i_{,k}+\tfrac{2}{3}g^{ij}\overline{u^ku_l}\,\underline{U}^l_{,k})}_{\text{due to Naot } et\ al.}.$$

Derivation of the above expressions, based on kinematic arguments, is given by Launder *et al.*[28] All constants are written as C with an associated subscript; the values used for turbulence constants in the present investigation are presented in Table III.

An inspection of the full Reynolds stress equations above shows that derivatives of the Reynolds stresses occur only in the convection and the diffusion terms. These terms may be modelled by assuming that the convection less diffusion of a Reynolds stress is proportional to the convection less diffusion of turbulent kinetic energy, in the ratio of the value of the stress to the value of the kinetic energy, suggested by Rodi,[21] giving the algebraic Reynolds stress equations

$$\begin{aligned}\overline{(u^ku_l\underline{U}^l_{,k}-\varepsilon)}\,\overline{u^iu^j}/k = &-\overline{u^iu^k}\,\underline{U}^j_{,k}-\overline{u^ju^k}\,\underline{U}^i_{,k}-C_1\varepsilon/k(u^iu^j-\tfrac{2}{3}g^{ij}k)\\ &-C_2(-\overline{u^iu^k}\,\underline{U}^j_{,k}-\overline{u^ju^k}\,\underline{U}^i_{,k}+\tfrac{2}{3}g^{ij}\overline{u^ku_l}\,\underline{U}^l_{,k})-\tfrac{2}{3}g^{ij}\varepsilon+(1-C_2)A^{ij}. \qquad (5)\end{aligned}$$

The addition of the term A^{ij} is to account for the fact that when the above equations are expressed in cylindrical co-ordinates for swirling flow, it is suggested that it is necessary to retain some of the convection terms and treat them as false production terms.[22,26] The convection terms retained are those associated with the Christoffel symbols, but since these are entirely a function of the co-ordinate system being used, they cannot be expressed in generalized co-ordinates and are therefore presented in Section 2.3. This is not satisfactory from the point of view of developing co-ordinate-system-independent turbulence models. Results obtained using the algebraic Reynolds stress model with and without the extra false production terms included have been obtained and are presented in Section 3.

Since with the above approximations the turbulent kinetic energy will appear explicitly in the Reynolds stress equations, it is also necessary to model terms in the k equation. The dissipation term has already been modelled above, and with the same assumption about the relative significance of the diffusion terms in high-Reynolds-number flow it is only necessary to model the $\overline{u^kk_{,k}}$ term, which is suggested to be proportional to the gradient of k:[17]

$$\overline{(u^kk)}_{,k} = g^{kl}(C_k\nu_{\text{eff}}k_{,k})_{,l}, \qquad (6)$$

where ν_{eff} is an effective viscosity equal to $\nu+\nu_t$, ν_t being the turbulent eddy viscosity given below.

The k equation may be written as

$$k_{,t}+\underbrace{\underline{U}^kk_{,k}}_{\text{convection}} = \underbrace{-\overline{u^ku_l}U^l_{,k}}_{\text{production}}+\underbrace{g^{kl}(C_k\nu_{\text{eff}}k_{,k})_{,l}}_{\text{diffusion}}-\underbrace{\varepsilon}_{\text{dissipation}}. \qquad (7)$$

It is still necessary to obtain an equation for ε, the scalar dissipation of k. An exact equation can be derived from the Navier–Stokes equations, but such drastic modelling assumptions have to be introduced that the resulting equation has a highly empirical character. Therefore it is assumed that a transport equation for ε similar to the k equation may be constructed by simply modifying

Table III. Turbulence constants

Turbulence model	Identifier	C_1	C_2	C_{k1}	$C_{\varepsilon 1}$	$C_{\varepsilon 2}$	$C_{\varepsilon 3}$	C_μ	κ
k–ε	k–ε	—	—	1·0	1·44	0·82	1·92	0·09	0·41
k–ε Plus Richardson correction factor	k–ε+R	—	—	1·0	1·44	0·82	1·92	0·09	0·41
Algebraic Reynolds stress	ARS	2·8	0·8	1·0	1·44	0·82	1·92	—	0·41
Algebraic Reynolds stress plus false production	ARS+FP	3·0	0·3	1·0	1·44	0.82	1·92	—	0·41

the terms in the k equation,[29] giving

$$\underbrace{\varepsilon_{,t}+\underline{U}^k\varepsilon_{,k}}_{\text{convection}}=\underbrace{C_{\varepsilon 1}\varepsilon/k(-\overline{u^k u^l}\underline{U}^l_{,k})}_{\text{production}}+\underbrace{g^{kl}(C_{\varepsilon 2}\nu_{\text{eff}}\varepsilon_{,k})_{,l}}_{\text{diffusion}}-\underbrace{C_{\varepsilon 3}\varepsilon^2/k}_{\text{dissipation}} \tag{8}$$

The correction to the ε equation to allow for the influence of swirl is a function of the local co-ordinate system and is presented in Section 2.4.

When the k–ε models are used, it is assumed that the turbulent stresses may be related to the rate of deformation tensor via an eddy viscosity, in a manner analogous to the viscous stresses, as

$$\overline{u^i u^j}=-\nu_t(g^{jk}\underline{U}^i_{,k}+g^{ik}\underline{U}^j_{,k})+\tfrac{2}{3}g^{ij}k. \tag{9}$$

The addition of $\frac{2}{3}g^{ij}k$ is to ensure that when the above equation is contracted on the free indices, the result is k, as otherwise it would be zero due to continuity. When the Reynolds stresses are substituted into the mean flow equations, this term is absorbed into the pressure and thus never appears explicitly.

The eddy viscosity is then related to the k and ε already calculated as

$$\nu_t=C_\mu k^2/\varepsilon. \tag{10}$$

2.3. *Turbulence models in physical co-ordinates*

To enable a solution to the equations given above to be obtained, they must be expressed in a suitable physical co-ordinate system. In the present case we have chosen to use spherical co-ordinates (Figure 1) as they conform naturally to the boundary of the physical domain and

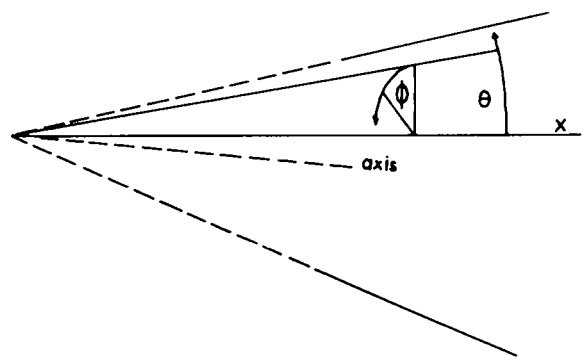

Figure 1. Spherical co-ordinate system

reduce flow-to-grid skewness when compared to cartesian or cylindrical co-ordinate systems.

Expressing the equations in physical co-ordinates is a straightforward, though tedious, process. The method to do this, as well as all of the equations, are given in Armfield.[5] In this paper we will present only those equations associated with the turbulence models, in particular to demonstrate the differences between the two k–ε models and the two algebraic Reynolds stress models, as these differences are very much a function of the co-ordinate system chosen.

The algebraic Reynolds stress equations (5) when written in spherical co-ordinates are

$\overline{uu}$ equation

$$\frac{(Pk-\varepsilon)\overline{uu}}{k}=\left[-2\overline{uu}U_x-2\overline{uv}\left(\frac{U_\theta}{x}-\frac{V}{x}\right)-2\overline{uw}\left(\frac{U_\phi}{x\sin\theta}-\frac{W}{x}\right)\right](1-C_2)$$
$$-\frac{C_1\varepsilon}{k(\overline{uu}-\frac{2}{3}k)}+C_2\tfrac{2}{3}Pk-\tfrac{2}{3}\varepsilon, \tag{11}$$

$\overline{vv}$ equation

$$\frac{(Pk-\varepsilon)\overline{vv}}{k}=\left[-2\overline{uv}V_x-2\overline{vv}\left(\frac{V_\theta}{x}+\frac{U}{x}\right)-2\overline{vw}\left(\frac{V_\phi}{x\sin\theta}-\frac{W\cot\theta}{x}\right)\right](1-C_2)$$
$$-\frac{C_1\varepsilon}{k(\overline{vv}-\frac{2}{3}k)}+C_2\tfrac{2}{3}Pk-\tfrac{2}{3}\varepsilon+2\frac{W}{x\tan\theta}\overline{vw}(1-C_2), \tag{12}$$

$\overline{ww}$ equation

$$\frac{(Pk-\varepsilon)\overline{ww}}{k}=\left[-2\overline{wu}W_x-2\overline{wv}\frac{W_\theta}{x}-2\overline{ww}\left(\frac{W_\phi}{x\sin\theta}+\frac{U}{x}+\frac{V\cot\theta}{x}\right)\right](1-C_2)$$
$$-\frac{C_1\varepsilon}{k(\overline{ww}-\frac{2}{3}k)}+C_2\tfrac{2}{3}Pk-\tfrac{2}{3}\varepsilon-2\frac{W}{x\tan\theta}\overline{vw}(1-C_2), \tag{13}$$

$\overline{uv}$ equation

$$\frac{(Pk-\varepsilon)\overline{uv}}{k}=\left[-\overline{uu}V_x-\overline{uv}\left(U_x+\frac{V_\theta}{x}+\frac{U}{x}\right)-\overline{vv}\left(\frac{U_\theta}{x}-\frac{V}{x}\right)\right.$$
$$\left.-\overline{uw}\left(\frac{V_\phi}{x\sin\theta}-\frac{W\cot\theta}{x}\right)-\overline{vw}\left(\frac{U_\phi}{x\sin\theta}-\frac{W}{x}\right)\right](1-C_2)-\frac{C_1\varepsilon\overline{uv}}{k}$$
$$+\frac{W}{x\tan\theta}\overline{uw}(1-C_2), \tag{14}$$

$\overline{uw}$ equation

$$\frac{(Pk-\varepsilon)\overline{uw}}{k}=\left[-\overline{uu}W_x-\overline{uw}\left(U_x+\frac{W_\phi}{x\sin\theta}+\frac{U}{x}+\frac{V\cot\theta}{x}\right)\right.$$
$$\left.-\overline{uv}\frac{W_\theta}{x}-\overline{vw}\left(\frac{U_\theta}{x}-\frac{V}{x}\right)-\overline{ww}\left(\frac{U_\phi}{x\sin\theta}-\frac{W}{x}\right)\right](1-C_2)-\frac{C_1\varepsilon\overline{uw}}{k}$$
$$-\frac{W}{x\tan\theta}\overline{uv}(1-C_2), \tag{15}$$

$\overline{vw}$ equation

$$\frac{(Pk-\varepsilon)\overline{vw}}{k}=\left[-\overline{uv}W_x-\overline{uw}V_x-\overline{vv}\frac{W_\theta}{x}-\overline{vw}\left(\frac{V_\theta}{x}+\frac{2U}{x}+\frac{W_\phi}{x\sin\theta}+\frac{V\cot\theta}{x}\right)\right.$$
$$\left.-\overline{ww}\left(\frac{V_\phi}{x\sin\theta}-\frac{W\cot\theta}{x}\right)\right](1-C_2)-\frac{C_1\varepsilon\overline{vw}}{k}$$
$$-\left(\frac{W}{x\tan\theta}\overline{vv}-\frac{W}{x\tan\theta}\overline{ww}\right)(1-C_2). \tag{16}$$

The false production terms associated with the Christoffel symbols and the convection terms, equation (5), have been included as the last term in each of the above equations (12)–(16) to allow them to be identified separately from the other terms.

2.3.1. Production of k. The term Pk which occurs in each of the above equations is the production of k; when expressed in spherical co-ordinates, it is given by

$$Pk=-\overline{uu}U_x-\overline{uv}\left(\frac{U_\theta}{x}-\frac{V}{x}\right)-\overline{uw}\left(\frac{U_\phi}{x\sin\theta}-\frac{W}{x}\right)-\overline{vv}\left(\frac{V_\theta}{x}+\frac{U}{x}\right)-\overline{vu}V_x$$
$$-\overline{vw}\left(\frac{V_\phi}{x\sin\theta}-\frac{W}{x\tan\theta}\right)-\overline{ww}\left(\frac{W_\phi}{x\sin\theta}+\frac{U}{x}-\frac{V}{x\tan\theta}\right)-\overline{wu}W_x-\frac{\overline{wv}W_\theta}{x}. \tag{17}$$

When we express the Reynolds stresses using the Boussinesq form, Pk becomes

$$Pk=\nu_t\left[2U_x^2+2\left(\frac{V_\theta}{x}+\frac{U}{x}\right)^2+2\left(\frac{W_\phi}{x\sin\theta}+\frac{U}{x}+\frac{V}{x\tan\theta}\right)^2\right.$$
$$\left.+\left(\frac{U_\phi}{x\sin\theta}-\frac{W}{x}+W_x\right)^2+\left(\frac{U_\theta}{x}-\frac{V}{x}+V_x\right)^2+\left(\frac{W_\theta}{x}+\frac{V_\phi}{x\sin\theta}-\frac{W}{x\tan\theta}\right)^2\right]. \tag{18}$$

2.4. k and ε equations

The k and ε equations must also be written in spherical co-ordinates, giving

k equation

$$Uk_x+\frac{Vk_\theta}{x}+\frac{Wk_\phi}{x\sin\theta}=Pk+C_k\left((\nu_{\text{eff}}k_x)_x+\frac{(\nu_{\text{eff}}k_\theta)_\theta}{x^2}+\frac{(\nu_{\text{eff}}k_\phi)_\phi}{x^2\sin^2\theta}+2\frac{\nu_{\text{eff}}k_x}{x}+\frac{\nu_{\text{eff}}k_\theta}{x^2\tan\theta}\right)-\varepsilon, \tag{19}$$

ε equation

$$U\varepsilon_x+\frac{V\varepsilon_\theta}{x}+\frac{W\varepsilon_\phi}{x\sin\theta}=\frac{C_{\varepsilon1}\varepsilon Pk}{k}+C_{\varepsilon2}\left((\nu_{\text{eff}}\varepsilon_x)_x+\frac{(\nu_{\text{eff}}\varepsilon_\theta)_\theta}{x^2}+\frac{(\nu_{\text{eff}}\varepsilon_\phi)_\phi}{x^2\sin^2\theta}+2\frac{\nu_{\text{eff}}\varepsilon_x}{x}+\frac{\nu_{\text{eff}}\varepsilon_\theta}{x^2\tan\theta}\right)-\frac{C_{\varepsilon3}\varepsilon^2}{k}. \tag{20}$$

A modification to allow for the influence of swirl is to multiply the constant $C_{\varepsilon3}$ in the above expression by the function $f_1=(1-0{\cdot}2Ri)$, where Ri is the gradient Richardson number:[14]

$$Ri=\frac{k^2}{\varepsilon^2}\frac{W}{x^2\sin^2\theta}(W\sin\theta)_\theta. \tag{21}$$

This correction is based on the hypothesis that the destabilizing effect of swirl can be modelled through an increase in the length scale of the turbulent eddies. It predicts a turbulence damping effect over large regions of the flow where $(W\sin\theta)_\theta$ is positive, leading to a reduction in the eddy viscosity.[14] In practice we constrain f_1 to not be greater than 2·80 and not less than 1·40 to prevent the dissipation becoming either too large or too small and affecting the stability of the scheme.

2.5. *Near-wall values for k and ε*

In the near-wall region the k and ε fields vary very rapidly, leading to large radial gradients.[30] To resolve such gradients, it is necessary to have an extremely fine mesh in this region. Additionally it has been demonstrated that the modelled form of the diffusion term in the k equation gives poor agreement with experimental data in the viscous region.[31] Therefore rather than integrate the k and ε equations to the wall, a near-wall point in the log-law region, at between a y^+ of 30 and 100, is chosen to be the computational boundary, and values for k and ε are obtained there from the following relations:

$$k_w=\frac{v_t^2}{l^2C_\mu^{1/2}}, \qquad \varepsilon_w=\frac{C_\mu^{3/4}k_w^{3/2}}{l}, \tag{22}$$

where k_w and ε_w are the near-wall values for k and ε respectively. We obtain v_t as

$$v_t=\frac{r}{R}l^2\left[\left(\frac{U_\theta}{x}\right)^2+\left(\frac{W_\theta}{x}-\frac{W}{x\tan\theta}\right)^2\right]^{1/2} \tag{23}$$

and

$$l=\kappa R\ln\frac{R}{r}\left[1-\exp\left(-R\ln\frac{r}{R}\frac{Re\tau_w^{1/2}}{A}\right)\right]. \tag{24}$$

In the above expression $A=26$, the wall shear stress τ_w is obtained using a first-order single-sided differencing of the velocity at the wall, R is the local diffuser radius, r is the radius at the near-wall point and κ is the von Karman constant, given in Table III. We have assumed here that the only significant terms in the near-wall region are U_θ/x and $W_\theta/x-W/x\tan\theta$.

2.6. *Boundary conditions*

To complete the mathematical specification of the problem, it is necessary, in addition to the governing equations, to provide appropriate boundary conditions. The boundary conditions used are as follows.

(1) *The diffuser entrance.* The U and W profiles are obtained from the experimental data; The V profile, if it is not given, is assumed to be zero. The turbulent kinetic energy k is when possible taken from the experimental data; otherwise it is obtained by assuming a turbulence kinetic energy as a percentage of total energy, typically 2%. ε at the entrance is assumed to obey the mixing length relation given in equation (22). The mixing length l is assumed to be 0·05 of the diffuser entrance diameter.

Although no differential equations are solved for the Reynolds stresses, due to the occurrence of the axial derivatives of $\overline{uu}$, $\overline{uv}$ and $\overline{uw}$ in the momentum equations, it is necessary to specify them at the entrance. To do this, it is assumed that their axial gradients are constant.

(2) *The axis.* From the axisymmetry of the flow we obtain that the θ gradients of U, k and ε are zero, and that V and W are zero. We must also specify the $\overline{vv}$, $\overline{vw}$ and $\overline{uv}$ Reynolds stresses. From experimental data it seems reasonable to set $\overline{vw}$ and $\overline{uv}$ to zero, and the θ gradient of $\overline{vv}$ to zero.[32]

(3) *The wall.* All velocities are set identically to zero; k and ε are obtained at a near-wall point from the formulations given in equation (22). Reynolds stresses are obtained at a near-wall point from the algebraic Reynolds stress equations when that model is being used.

(4) *The exit.* All axial gradients are set to zero.

The normal gradient of the pressure is set to zero on all boundaries, except the wall, where it is obtained directly by enforcing a mass flow constraint.[16]

2.7. Numerical scheme

In this scheme, described in detail in Armfield and Fletcher,[16] the domain is discretized in the manner indicated in Figure 2, with all variables stored at all locations in the domain. Each dependent variable is obtained sequentially from its own equation, the remaining dependent variables in that equation being obtained from the stored solutions. The new values of each variable are then used to relax the stored solutions. To provide an initial solution, it is assumed that those variables given at the diffuser entrance are constant for the entire domain while the remaining variables are set to zero.

The pressure is treated as a special variable. Thus while all the other variables are obtained, and the stored solutions relaxed, in a single sweep in a manner very similar to that used in the single-sweep scheme, the pressure is obtained from a Poisson equation making several sweeps of the domain while the values of all other variables are held fixed. Convective terms are differenced using a hybrid central/upwind scheme, with all other terms centrally differenced.

The multi-sweep scheme is the only scheme of those indicated in Table II that can solve the full equations with no minimum step size stability restriction but which can also be used to solve the partially reduced and the reduced equations.

3. RESULTS

The multi-sweep scheme described in Section 2.7 has been run on a Perkin-Elmer 3220 computer. Results presented are for an axial step size of 0·1 of the entrance diameter, with a non-constant

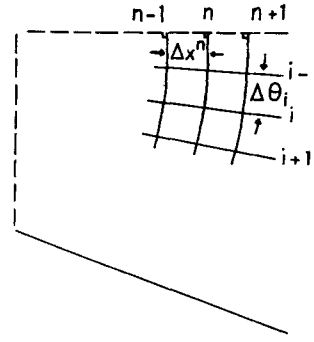

Figure 2. Discretization

mesh of 40 points in the radial direction. The point nearest the wall is located 0·001 of a diameter from the wall, while that nearest the axis is 0·02 of a diameter from the axis. Exponential stretching is used to increase the mesh size in the region away from the axis and the wall; the maximum change in grid size is 10%. Relaxation factors are 0·4 for all non-turbulence quantities and 0·2 for the turbulence quantities. Convergence is assumed when the maximum change in any field between one iteration and the next is less than 0·0001. This leads to convergence for the k–ε models in 400 iterations and for the algebraic Reynolds stress models in 600 iterations. Run times on the Perkin-Elmer are of the order of 30 s per iteration. The values used for the turbulence constants are listed in Table III.

3.1. Results of Clausen

The experimental data of Clausen[33] consist of results for swirling flow in a conical diffuser of 20° total internal angle, with an area ratio of four, at a Reynolds number of 200 000, exhausting into the atmosphere. Swirl is generated by a rotating cylinder packed with axially oriented straws placed about one diameter upstream of the diffuser entrance. This has the effect of producing an inlet swirl profile of solid body rotation type, the magnitude of which may be varied by changing the speed of rotation of the cylinder, with close-to-uniform axial velocity in the core region.

The experimental results presented are for the moderate swirl regime ($Sn = 0{\cdot}5$), with no axial velocity reversal either at the centreline or the wall. Without the inclusion of swirl the diffuser angle is such that separation at the wall takes place. In fact the level of swirl considered here is the only one that for this diffuser leads to no separation or reversal. Inclusion of any more swirl has been found to lead to centreline axial velocity reversal; any less leads to separation at the wall.[33] Clausen presents intial profiles for all mean velocities and for k which are used for the computation; the intial ε profile is estimated in the manner indicated in Section 2.6.

Figure 3 presents the results for the axial velocity obtained using the k–ε, the k–ε+R, the ARS and the ARS+FP turbulence models, compared with the data of Clausen, at a point half a diameter upstream from the diffuser exit. As can be seen, all the models lead to qualitatively satisfactory agreement, clearly predicting the overall reduction in velocity associated with the

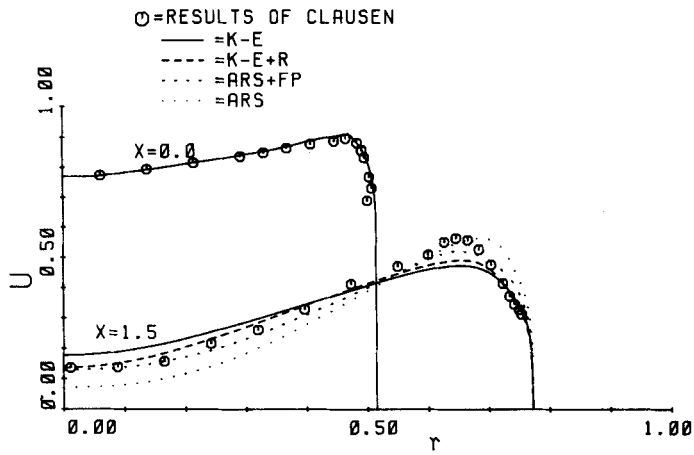

Figure 3. Axial velocity using ARS, ARS+FP, k–ε and k–ε+R models compared with data of Clausen

constant mass flow as well as the effect of swirl in reducing the centreline and increasing the near-wall axial velocity proportionally. The two algebraic Reynolds stress models perform better than the k–ε models, which both underpredict the magnitude of the near-wall velocity peak. Of the two k–ε models the k–ε+R gives the better prediction, accurately predicting the centreline velocity and not underpredicting the near-wall velocity peak by as much. The ARS+FP would appear to be slightly better than the ARS model. The ARS does predict the near-wall velocity peak more accurately, but places it too close to the wall and underestimates the centreline axial velocity.

Figure 4 indicates the radial profiles for the swirl velocity. Once again the two algebraic Reynolds stress models give better prediction than the k–ε models, with the latter giving very close to solid body rotation and underpredicting the magnitude of the near-wall velocity peak. Both algebraic Reynolds stress models predict the dip below solid body rotation of the experimental points very well, although both fail to match the very high level of swirl at the near-wall point. It is possible that there may be some experimental inaccuracy in the measurement of the near-wall swirl velocity, as the apparent non-existence of any boundary layer at the downstream location seems unusual. It is very difficult to say which of the algebraic Reynolds stress models is better; the ARS may be slightly better because of its more accurate prediction of the near-wall velocity peak. There appears to be very little difference between the two k–ε models for the swirl velocity.

Figure 5 shows the eddy viscosity distributions associated with the ARS and ARS+FP models, obtained from the $\overline{uv}$ and $\overline{vw}$ stresses, compared with those obtained with the k–ε and k–ε+R models. The experimental eddy viscosities have been extracted from the experimental data and can be taken as an indication only, being subject to a great deal of error. Nonetheless, it is apparent that the experimental results indicate that the assumption of isotropy is not correct for this type of flow.

We see that the k–ε model predicts an eddy viscosity that falls somewhere between the experimental eddy viscosities, and that inclusion of the Richardson correction factor reduces its magnitude quite substantially. This results in an improved approximation to the axial eddy viscosity, but a worse approximation to the swirl eddy viscosity.

The ARS model predicts anisotropic eddy viscosities, but as can be seen, there is very little difference between the axial eddy viscosity and the swirl eddy viscosity. The predicted swirl eddy viscosity is larger than the axial eddy viscosity, which is the same as the experimental data. Consequently the swirl eddy viscosity is considerably underpredicted, whilst the axial eddy

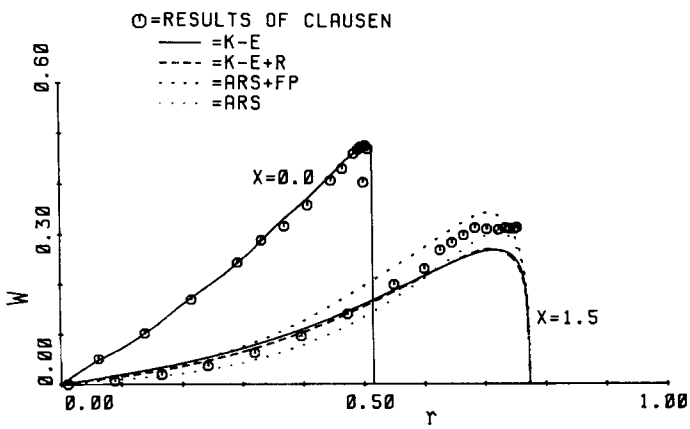

Figure 4. Swirl velocity using ARS, ARS+FP, k–ε and k–ε+R models compared with data of Clausen

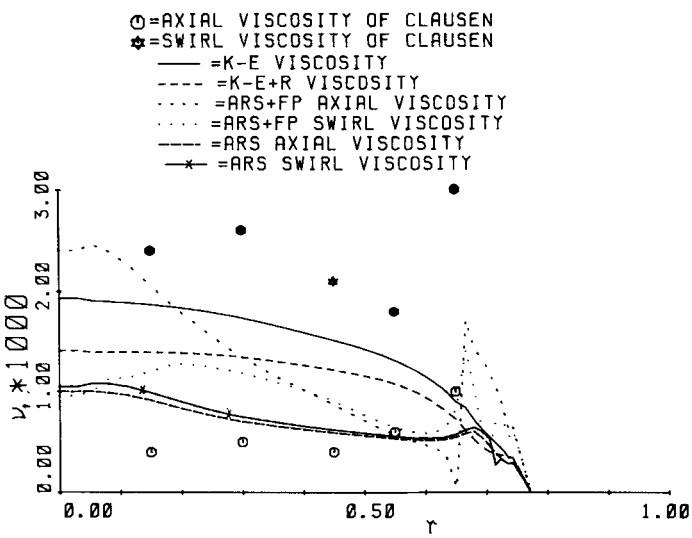

Figure 5. Eddy viscosities obtained using the ARS, ARS + FP, k–ε and k–ε + R models compared with results of Clausen

viscosity is predicted more accurately than by any other model. The ARS + FP model predicts far more anisotropy in the eddy viscosities than the ARS model; unfortunately the change is in the wrong direction, with the axial eddy viscosity larger than the swirl, the opposite to the experimental data. We also see that the ARS + FP model leads to a very uneven prediction; the ARS + FP model has been found to be in general less stable than the ARS model, and this is a reflection of that instability.

Figures 6 and 7 demonstrate that the axial development of the axial and swirl velocities, using the ARS model, is in good agreement with the experimental results. The predictions are somewhat better at the upstream locations.

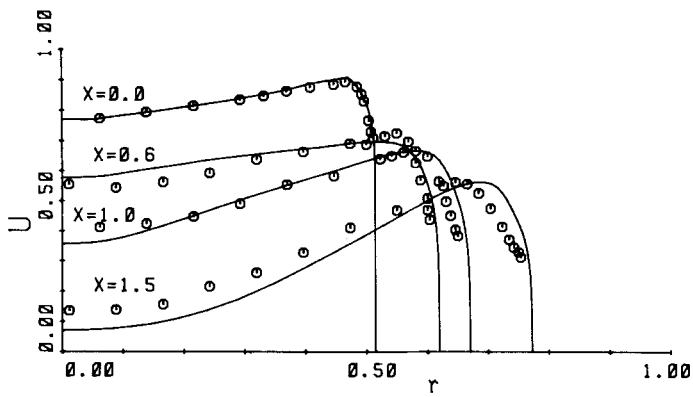

Figure 6. Development of axial velocity using ARS compared with data of Clausen

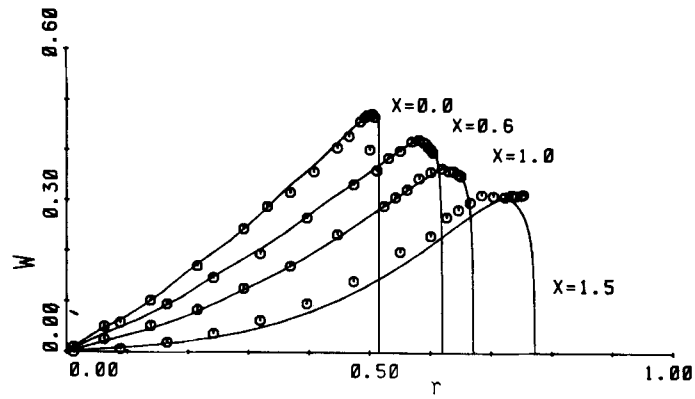

Figure 7. Development of swirl velocity using ARS compared with data of Clausen

3.2. *Results of Okwuobi and Azad*

Okwuobi and Azad[34] present results for non-swirling flow in a conical diffuser of 8° internal angle, with an area ratio of four, discharging into the atmosphere. The entrance profiles are those of fully developed pipe flow, with the axial velocity very close to separation at the diffuser exit; the Reynolds number is 250 000. This flow has been simulated using the multi-sweep algorithm with the ARS turbulence model.

Although the flow is non-swirling, it is considered useful to present these results to enable the prediction of the turbulent quantities to be examined more closely. Figures 8, 9 and 10 contain the results for the axial velocity, the turbulence kinetic energy and the $\overline{uv}$ stress respectively, obtained using the ARS model with the standard constants (Table III), and using the ARS model with C_{k1} set to 0·50 and κ set to 2·00. Thus we have halved the gradient diffusion of k and increased the predicted length scale at the near-wall point by five times. Why we should choose to adjust these constants is discussed in the next section.

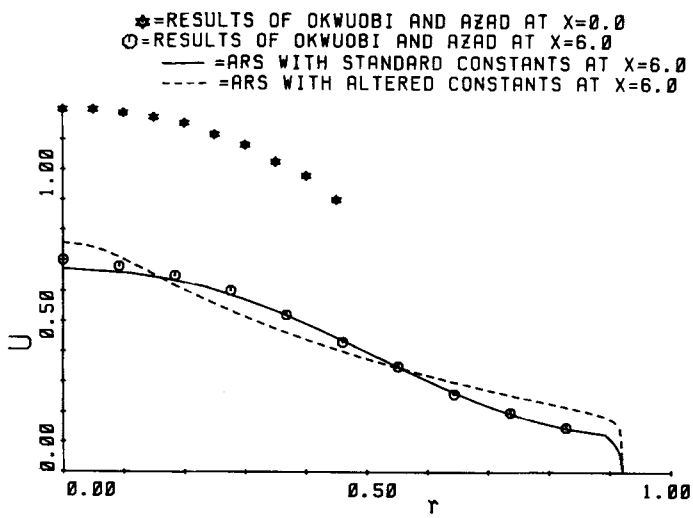

Figure 8. Axial velocity using ARS model compared with data of Okwuobi and Azad

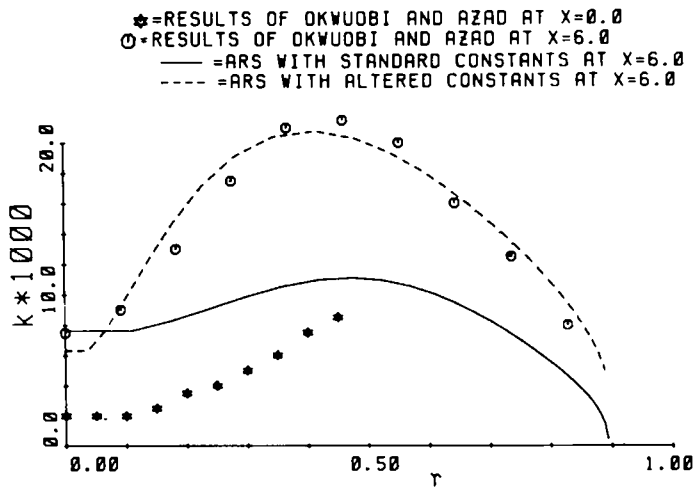

Figure 9. k using ARS model compared with data of Okwuobi and Azad

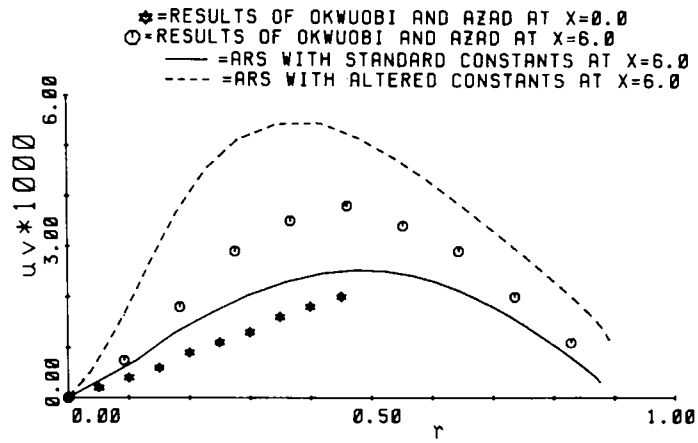

Figure 10. $\overline{uv}$ using ARS model compared with data of Okwuobi and Azad

If we first consider the results obtained using the standard constants, we see that the mean velocity is very well predicted but the k and $\overline{uv}$ quantities are seriously underpredicted. The peak in both of the turbulent profiles has remained at a radial location of 0·5, which means that it has simply travelled straight on from the diffuser entrance rather than turning around the corner. It can be seen that the algorithm does predict the existence of these peaks but significantly underestimates them. At the near-wall point where k is obtained using the local equilibrium assumption it is underpredicted by around 75% and the predicted profile is too flat.

As can be seen, by altering the constants we have obtained a much better prediction for k (Figure 9). Unfortunately the prediction of the mean velocity is now degraded, as can be seen from Figure 8, and the predicted $\overline{uv}$ profile (Figure 10) has been increased too much.

4. DISCUSSION

The use of hybrid central/upwind differencing schemes of the type employed in the present multi-sweep scheme is a potential source of inaccuracy due to the possible numerical diffusion.[35] In the flows considered in the present investigation the axial velocity is large enough so that at most points of the flow upwind differencing is used for the axial convective term; the cross-stream velocity is small so that central differencing is used at most points of the domain for the radial convective term. This raises the question of whether large numerical diffusion is resulting from the first-order differencing of the axial convection terms. In the present investigation we have only considered non-reversing flows in which the axial diffusion is relatively small. In addition we have used grids that have been demonstrated fine enough to lead to numerical diffusion-free solutions even for highly recirculating turbulent flow using a similar first-order upwind differencing scheme.[36] It is therefore suggested that numerical diffusion is not having a significant effect on the solutions presented.

4.1. Turbulence models

For the flow of Clausen all of the turbulence models give satisfactory qualitative predictions of the mean velocities, with the two algebraic Reynolds stress models giving better prediction of the fine detail. In particular they predict the drop below solid body rotation of the swirl profile very well, which is not well predicted by the k–ε models, and more accurately predict the axial centreline velocity and the magnitude of the near-wall velocity peak for both axial and swirl velocities (Figures 3 and 4). The inclusion of the Richardson correction factor, described in Section 2.4, does lead to a slight improvement for the axial velocity prediction, but makes very little difference to the swirl velocity.

The axial velocity for the non-swirling flow of Okwuobi and Azad (Section 3.2) is predicted very well using the ARS model. No detailed comparison of the turbulence models with each other has been made for this data set, as results were computed primarily to test the validity of the near-wall local equilibrium assumption (Section 2.5) and the effect of adjusting the diffusion parameter in the k equation. These features are common to both the ARS and k–ε models. For the non-swirling flow of Okwuobi and Azad, including a Richardson number correction factor in the k–ε model, or false production terms in the ARS model, has no effect.

As has been demonstrated, it appears that by using a suitable model it is possible to obtain reasonable predictions for the mean flow, even though, as has been demonstrated in the flow of Clausen, the prediction of the eddy viscosity is rather poor. From the results (Figure 5) it is apparent that the eddy viscosities are anisotropic, with the swirl viscosity far larger than the axial viscosity. None of the turbulence models satisfactorily represents this anisotropy. The k–ε model predicts an eddy viscosity that is too large for the axial viscosity and too small for the swirl viscosity. Inclusion of the Richardson correction factor reduces that viscosity to bring it more into line with the axial viscosity. It would appear therefore that it is more important to predict the axial viscosity than the swirl viscosity, as the Richardson correction improves the prediction of mean flow quantities compared to the standard k–ε model. This is in agreement with the observed fact that the centreline axial velocity is the most sensitive parameter. The ARS model predicts an axial viscosity that is closer to the experimental value than either of the k–ε models, but predicts a swirl viscosity that is so close to the axial that it may as well be isotropic. The ARS + FP model predicts substantial anisotropy but in the wrong direction. Thus neither of the algebraic Reynolds stress models satisfactorily accounts for the anisotropy, and it appears that of the two viscosities it is more important to correctly predict the axial viscosity, which the ARS model does more accurately in the core region than the ARS + FP, k–ε and k–ε + R models.

Although constructing an equivalent eddy viscosity from an ARS formulation is artificial, and certainly not an inherent part of the model, it is nonetheless felt that this is a valuable additional means of comparing the results with those of an eddy viscosity model. If the comparison is only made at the Reynolds stress level, it is possible that the mean velocity field may modify some feature in the eddy viscosity model that is primarily due to the eddy viscosity construction. It is suggested that the additional comparison at the eddy viscosity level allows more complete conclusions to be drawn.

Considering the non-swirling flow of Okwuobi and Azad, we see that the magnitude of the turbulence quantities is severely underpredicted using the standard constants, and we also see that the peak is now some distance from the wall, at $r=0{\cdot}5$, at the downstream location. This is the radius of the diffuser entrance, and what appears to have happened is that the near-wall peak in k and $\overline{uv}$ has carried straight on down the diffuser, so that by the exit it is well away from the wall and has increased significantly. Behaviour of this sort is not characteristic of attached boundary layers, for which the near-wall peak is, in the case of pipe flow at high Reynolds numbers, within 0·01 of a diameter of the wall. We do see behaviour of this sort in separating and nearly separating boundary layers,[37,38] suggesting that the turbulent structure of diffuser flow may be similar to that of a two-dimensional boundary layer approaching a separation point.

Two groups of researchers who have attempted to simulate the turbulence quantities in separating boundary layers are Johnson and Horstman[37] and Viegas *et al.*[38] Johnson and Horstman, using a two-equation k, $k^{1/2}L^{-1}$ model integrated to the wall, present results showing that the peak in turbulence quantities, which has moved away from the wall, is underestimated by around 70% at the separation point. Viegas *et al.* compare results obtained using a wall function approach, and a k–ε model integrated to the wall, to simulate a separating boundary layer, and once again the peak, which has moved away from the wall, is being underestimated by both methods. On these bases we suggest that the experimental phenomenon observed in the diffuser is similar to that associated with separating two-dimensional boundary layers, and that it appears that neither wall functions nor two-equation models integrated to the wall can model the turbulence structure near to such a region in a completely satisfactory manner.

Okwuobi and Azad present results demonstrating that their flow is not a log-law flow and does not have a region of local equilibrium. However, we obtain a near-wall boundary value for k by assuming that the flow is in local equilibrium, which, if this is not so, will lead to an inaccuracy. It might appear that integrating the equations to the wall, if the computer resources are available, rather than using a local equilibrium assumption, would correct this discrepancy. Both Johnson and Horstman and Viegas *et al.* present results obtained by integrating to the wall, and still underpredict the turbulent peaks by a significant amount. To suggest what the other problem may be, we refer to a paper by Bernard,[31] who demonstrates that for fully developed channel flow the near-wall peak in k is underpredicted by around 25% when the k equation is integrated to the wall, even with the inclusion of near-wall correction factors. He suggests that it is the modelled form of the diffusion term that is primarily responsible for this underprediction. It could well be that a similar, though more severe, phenomenon is observed when the k equation is integrated to the wall for separating diffuser flow.

This led us to suppose that by altering those constants associated with the diffusion of k, and obtaining k at a near-wall point using the local equilibrium assumption, we may obtain an improvement. To test this hypothesis, we tried simulating the Okwuobi and Azad data with, firstly, the von Karman constant (κ) set to 2·00, five times its normal value. By doing this, we expected to increase the near-wall boundary value for k obtained from the local equilibrium relation. The result was to increase the near-wall k value as expected, but the peak was still underpredicted due to the lack of curvature in the profile. Decreasing C_{k1} to 0·50 (decreasing the

gradient diffusion of k by a half) increased the curvature of the k profile sufficiently to enable (with the altered von Karman constant) the k profile to be predicted very well at the downstream location (Figure 9). Unfortunately at the same time the mean flow velocity prediction is less satisfactory (Figure 8) and $\overline{uv}$ is now overpredicted (Figure 10). This is not too surprising, since although we may have chosen a new set of constants that are more valid for separating flow, at the diffuser entrance where the flow is not close to separation these constants are not valid. Nonetheless, the result does give support to the hypothesis that the poor prediction of turbulence quantities in the Okwuobu and Azad flow is related to the invalidity of the local equilibrium assumption and poor modelling of the k diffusion term. Physically we can interpret these results as indicating that the production of turbulence in the diffuser flow in the near-wall region is larger than in fully attached flow, and that the diffusion of k in the region of the peak is smaller than that predicted with the normal constant.

When a wall echo effect similar to that given by Sloane *et al.*[29] is included in the pressure strain approximation, it is found to produce almost identical mean velocity profiles. Although it does damp the near-wall peak in $\overline{vv}$, as it is designed to, it does not improve the prediction of the near-wall peak in the turbulent quantities. Therefore it appears that the use of a mixing length formulation in the near-wall region tends to minimize any contribution from the modelling of the wall echo effect. If the ARS turbulence model is used right up to the wall, it is likely that modelling of the wall echo effect will be more important.

5. CONCLUSIONS

To enable comparison and development of turbulence models for swirling diffuser flows, it is essential that a suitable set of experimental data is available. These data must consist of detailed measurements of the inlet profiles, both mean and turbulent, and profiles at several axial locations in the diffuser.

It is suggested that to obtain satisfactory predictions for the mean flow when moderate swirl is present, the standard k–ε model is not satisfactory, and the Richardson number correction used in the present investigation, although it leads to some improvement, is not adquate. Further *ad hoc* modifications could be made to improve the k–ε model for these flows, but it is felt that the use of a Reynolds stress model is a more satisfactory approach. The reason the k–ε model gives unsatisfactory predictions is that it predicts an eddy viscosity that is much larger than the experimental axial eddy viscosity, which is the more important of the two considered. The Richardson correction factor improves this by reducing the eddy viscosity, primarily by increasing the dissipation.

The two algebraic Reynolds stress models used in the present investigation both provide better prediction of the mean flow quantities than the k–ε models. Of the two the ARS is preferred because it gives a better prediction for the eddy viscosities, providing a more accurate approximation to the axial viscosity than the ARS+FP, which actually predicts the anisotropy in the wrong direction.

The results for the eddy viscosities are very disappointing, with the anisotropy basically not being predicted at all by either the ARS or the ARS+FP models. Since prediction of the anisotropy is the main reason for using the algebraic Reynolds stress models, this is unfortunate. They do appear to predict the effect of the swirl on dampening the level of turbulence better than the k–ε model. It is suggested that to determine if the algebraic approximation may be leading to loss of the anisotropy, and to determine which algebraic Reynolds stress approach is really better, it is necessary to compare the results obtained using the algebraic formulations with those obtained using a full Reynolds stress formulation.

The modelling of the length scale in the near-wall region and the modelling of the diffusion term in the k equation appear to be unsatisfactory for near-separating flows of the type found in diffusers. As has been demonstrated, the standard constants associated with these modelling assumptions do not accurately represent the behaviour of the diffuser flow at downstream locations, where it is close to separation. It may be necessary to make these constants functions of the axial location in order to suitably represent the apparent change in their value as the flow passes down the diffuser. Such an approach is currently being tested.

ACKNOWLEDGEMENT

The authors are grateful to the Australian Research Grants Committee for the support given to this research.

REFERENCES

1. C. A. J. Fletcher, A. J. Honan and J. S. Sapupo, 'Aerodynamic platform comparisons for jet-stream electricity generation', *J. Energy*, **7**, 17–23 (1983).
2. C. A. J. Fletcher and B. W. Roberts, 'Electricity generation from jet-stream winds', *J. Energy*, **3**, 241–249 (1979).
3. G. Sovran and E. Klomp, *Fluid Mechnaics of Internal Flow*, Elsevier, 1967.
4. Y. Senoo, N. Kawaguchi and T. Nagata, 'Swirl flow in conical diffusers', *Bull. JSME*, **21**, 112–119 (1978).
5. S. Armfield, 'Numerical simulation of turbulent swirling flow in conical diffusers', *Ph. D. thesis*, University of Sydney, 1987.
6. S. W. Armfield and C. A. J. Fletcher, 'Numerical simulation of swirling diffuser flow', *Int. j. numer. methods fluids*, **6**, 541 556 (1986).
7. S. W. Armfield and C. A. J. Fletcher, 'Pressure related instabilities of reduced Navier–Stokes equations', *Commun. Appl. Numer. Methods*, **2**, 377–383 (1986).
8. S. W. Armfield and C. A. J. Fletcher, 'A comparison of single and multi-sweep techniques for reduced Navier–Stokes equations', in J. Noye and R. May (eds), *Computer Technology and Applications CTAC 85*, North-Holland, Amsterdam, 1986, pp. 431–442.
9. A. D. Gosman and W. M. Pun, 'Calculation of recirculation flows', *Report HTS/74/2*, Department of Mechanical Engineering, Imperial College, 1974.
10. S. V. Patankar and D. B. Spalding, 'Three dimensional parabolic flow', *Int. J. Heat Mass Transfer*, **15**, 1787–1796 (1972).
11. I. Kubo and F. C. Gouldin, 'Numerical calculations of turbulent swirling flow', *ASME J. Fluids Eng.*, **97**, 310–315 (1975).
12. D. L. Rhode, D. G. Lilley and D. K. McLaughlin, 'On the prediction of swirling flow fields found in axisymmetric combustor geometries', *ASME J. Fluids Eng.*, **104**, 378–384 (1982).
13. C. Hah, 'Calculation of various diffuser flows with inlet swirl and inlet distortion effects', *AIAA J.*, **21**, 1127–1133 (1983).
14. M. A. Leschziner and W. Rodi, 'Computation of strongly swirling axisymmetric free jets', *AIAA J.*, **22**, 1742–1747 (1984).
15. J. S. Truelove and T. Mahmud, 'Calculation of strongly swirling jet flows', *9th Australasian Fluid Mechanics Conf.*, Auckland, 8 12 December 1986, pp. 492–499.
16. S. W. Armfield and C. A. J. Fletcher, 'A multi-sweep scheme for internal swirling flow in conical diffusers', (submitted 1989).
17. T. Cebeci and A. Smith, *Analysis of Turbulent Boundary Layers*, Academic Press, 1974.
18. M. A. Habib and J. H. Whitelaw, 'The calculation of turbulent flow in wide angle diffusers', *Numer. Heat Transfer*, **5**, 145–164 (1982).
19. B. E. Launder, C. H. Priddin and B. I. Sharma, 'The calculation of turbulent boundary layers on spinning and curved surfaces', *ASME J. Fluids Eng.*, **99**, 231–239 (1977).
20. D. Lilley, 'Prediction of inert turbulent swirl flows', *AIAA J.*, **11**, 955–960 (1973).
21. W. Rodi, 'A new algebraic relation for calculating the Reynolds stresses', *ZAMM*, **56**, 219–221 (1976).
22. M. L. Koosinlin and F. C. Lockwood, 'The prediction of axisymmetric turbulent swirling boundary layers', *AIAA J.*, **12**, 547–554 (1974).
23. P. Y. Chou, 'On velocity correlations and the solution of the equations of turbulent fluctuations', *Q. J. Appl. Math.*, **3**, 38–54 (1945).
24. J. C. Rotta, 'Statische theorie nichthomogener turbulenz', *Z. Phys. Bd.*, **192**, 547–572 (1968) and *Bd.*, **131**, 51–77 (1951) (English translation: *Report TM/TN/A/16*, Department of Mechanical Engineering, Imperial College, 1968).
25. D. Naot, A. Shavit and M. Wolfshtien, 'Interactions between components of the turbulent velocity correlation tensor due to pressure fluctuations', *Israel J. Technol.*, **8**, 259–269 (1970).

26. M. M. Gibson and B. A. Younis, 'Calculation of swirling jets with a Reynolds stress closure', *Phys. Fluids*, **29,** 38–48 (1986).
27. B. Launder, 'Turbulence modelling—a preview', *Colloq. on Computational Fluid Dynamics*, University of Manchester Institute of Science and Technology, 21–22 April 1986.
28. G. E. Launder, G. J. Reece and W. Rodi, 'Progress in the development of a Reynolds stress turbulence closure', *J. Fluid Mech.*, **68,** 537–566 (1975).
29. K. Hanjalic and B. E. Launder, 'A Reynolds stress model of turbulence and its application to thin shear flows', *J. Fluid Mech.*, **52,** 609 (1972).
30. P. Virenda, W. Rodi and G. Scheurer, 'Turbulence models for near wall and low Reynolds number flows: a review', *AIAA J.*, **12,** 1308–1319 (1985).
31. P. S. Bernard, 'Limitations of the near wall k–ε model', *AIAA J.*, **21,** 619–622 (1986).
32. J. Sislian and R. Cusworth, 'Measurements of mean velocity and turbulence intensities in a free isothermal swirling jet', *AIAA J.*, **24,** 303–309 (1986).
33. P. Clausen, 'Measurement and predictions of swirling flow behind turbine blades and through axisymmetric diffusers', *Ph. D. thesis*, University of Newcastle, Australia, 1987.
34. P. Okwuobi and R. Azad, 'Turbulence in a conical diffuser with fully developed flow at entry', *J. Fluid Mech.*, **57,** 603–622 (1973).
35. B. Leonard, in C. Taylor and K. Morgan (eds), *Computational Techniques in Transient and Turbulent Flow, Vol. 1*, Pineridge Press, Swansea, 1981.
36. J. McGuirk, A. Taylor and J. Whitelaw, 'The assessment of numerical diffusion in upwind difference calculations of turbulent recirculating flows', in *Turbulent Shear Flows 3*, Springer-Verlag, 1981, pp. 206–224.
37. D. Johnson and C. Horstman, 'Comparison between experiment and prediction for a transonic turbulent separated flow', *AIAA J.*, **20,** 737–744 (1982).
38. J. Viegas, M. Rubesin and C. Horstmann, 'On the use of wall functions as boundary conditions for two dimensional separated compressible flows', *AIAA' 85, AIAA 23rd Aerospace Science Meeting*, Reno, Nevada, 1985.
39. D. G. Sloan, P. J. Smith and D. Smoot, 'Modelling of swirl in turbulent flow systems', *Proc. Energy Comb. Sci.*, **12,** 163–250 (1986).